Available online at www.sciencedirect.com
ScienceDirect
Infrared Physics & Technology 50 (2007) 113–118
INFRARED PHYSICS & TECHNOLOGY
www.elsevier.com/locate/infrared

Van Hove singularities in intersubband transitions in multiquantum well photodetectors

J. Le Rouzo [a,*], I. Ribet-Mohamed [a], R. Haidar [a], M. Tauvy [a], N. Guérineau [a], E. Rosencher [a,b], S.L. Chuang [c]

[a] ONERA, Chemin de la Hunière, 91761 Palaiseau, France
[b] Ecole Polytechnique, Palaiseau, France
[c] University of Illinois, Department of Electrical and Computer Engineering, 1406 W. Green Street, Urbana, IL 61801, United States

Available online 14 November 2006

Abstract

High dynamics measurements of spectral response were carried out on quantum well infrared photodetectors (QWIP). Photocurrent spectra were studied over more than three orders of magnitude, revealing the presence of spectral structures which were never observed hitherto. Electric field assisted tunneling and, more surprisingly, Van Hove singularities at the miniband edges, are shown to play an important role in the low and high energy parts of the QWIP photocurrent spectra, respectively. These experimental features motivated us to initiate a theoretical study of the absorption in a multiquantum well structure. Our work is based on the study of the electronic wave function in a periodic structure.

PACS: 42.50.Ct; 85.60.Gz

Keywords: Quantum well infrared photodetectors; Photocurrent spectra; Van Hove singularities; Electric field assisted tunneling

1. Introduction

Multiquantum well infrared photodetectors (QWIPs) are now a mature technology, for large infrared focal plane arrays [1–4]. One of the potential of this technology, is the possibility of multispectral detection, thanks to stacked structures with different growth parameters [5]. For this purpose, it is very important to determine and understand the photoresponse of QWIPs with a great accuracy far from their peak responsivity. Indeed, this will allow one to evaluate the possible cross talk between the signals originating from different detected infrared bands (3–5 μm and 8–12 μm for instance). However, mainly because of experimental difficulties, very little effort has been devoted to measure and modelling these off-band responsivities with sufficient dynamical range. In this article, we describe an experiment (referred as Log spectra in the text) which allows these measurements. Thanks to the large dynamical range, these Log spectra show that the off band spectral responsivity of QWIPs is largely influenced by quantum effects such as electric field assisted tunnelling for the low energy side and, rather unexpectedly, by Van Hove singularities due to the quantum well periodicity for the high energy side.

Section 2 describes the test bench dedicated to the spectral response measurements and the detectors under study. The experimental results are then compared to our model, based on a Kronig–Penney approach (see Section 3.1).

2. Experimental photocurrent spectra of a single element QWIP

2.1. Experimental setup

Fig. 1 presents the technique developed at ONERA to perform spectral studies. It is based on the use of a

* Corresponding author. Tel.: +33 1 69 93 63 38; fax: +33 1 69 93 63 45.
E-mail addresses: lerouzo@onera.fr, Judikael.Le_Rouzo@onera.fr (J. Le Rouzo).

1350-4495/$ - see front matter © 2006 Elsevier B.V. All rights reserved.
doi:10.1016/j.infrared.2006.10.016

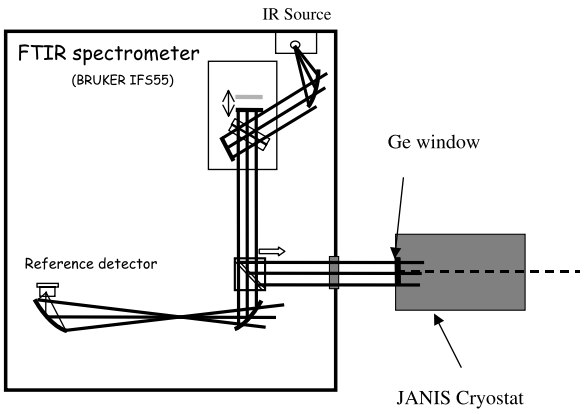

Fig. 1. ONERA experimental setup for the measurements of spectral response.

commercial FTIR spectrometer. The QWIP is mounted in a JANIS continuous flow helium cryostat placed outside a Fourier transform infrared spectrometer (FTIR). The commercial FTIR (Bruker, Equinox IFS55) produces either a reference spectrum (thanks to an internal reference detector with a known spectral response), or an external collimated beam of uniform intensity which is used to illuminate the detector. The angle of incidence on the sample may be adjusted from normal incidence to ±50° [6]. In fact the detector is put on a cold disc which is tilted with respect to the coldfinger with an angle of 50° in order to increase the signal noise ratio (see Fig. 2). The time-dependent signal delivered by the detector in response to the time-varying interferogram is amplified (Keithley 428) and sent to a series of pass-band filters to get rid of noise. It is then sent to the spectrometer for Fourier transformation and normalization by the reference spectrum. The spectral emission of the internal source, the reference detector response and the transmission of the cryostat germanium window are taken into account in our measurements.

Limiting the experimental noise is a crucial issue in such high dynamics measurements. Therefore, all electrical wires are protected inside and outside the cryostat. Thus we can assure a low noise experimental setup. The repeatability of our measures also indicates that the features observed on the QWIP spectral response are not artefacts.

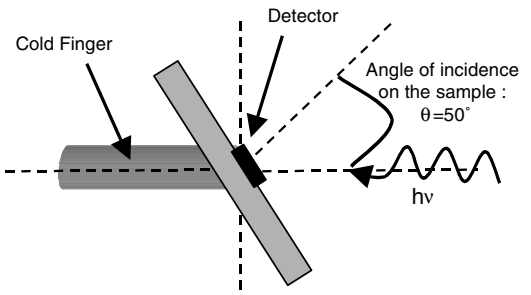

Fig. 2. Position of the detector in the cryogenic assembly.

2.2. Samples under study and operating conditions

The measurements presented in this paper were realized on QWIP single elements provided by Thales – Research and Technology laboratory. The peak wavelength of the 100 μm × 100 μm pixels is 8.5 μm. They consist in 40 GaAs quantum wells, 5 nm thick with 35 nm $Al_{0.26}Ga_{0.74}As$ barriers. The structure was designed so that the first excited state is quasi-bound in the well. The following results would nevertheless apply to bound-to-extended transitions. Bound to bound transitions are more complex because of additional phenomena, such as sequential tunnelling [7]. Mesas are defined by reactive ion etching. In order to determine the intrinsic spectral responsivity of the QWIPs, we worked with samples without any grating coupling.

The photodetectors are located on the coldfinger of the cryogenic assembly (see Fig. 2). Although the typical operating temperature is 70–75 K [8] for this kind of components in high performance cameras, we resorted to use a lower operating temperature of 40 K for our experiment, in order to decrease the dark current.

2.3. Experimental results

Fig. 3 shows the Log spectra of QWIPs for different applied biases. For comparison purpose, the spectra are normalized to their peak responsivities. This figure illustrates the good dynamical range of our measurements since three orders of magnitude are explored thanks to our low noise experimental setup. The main features of the figures are the following: Firstly, the experiment confirms the non negligible off-band response of the QWIP in the 3–5 μm window compared to its resonance value (still 1% in the 3–5 μm range). This value, however, is likely to be attenuated using coupling gratings. Secondly the low energy side of the spectral response is strongly affected by the applied electric field while the high energy side shows little dependence. Finally, rather sharp features are

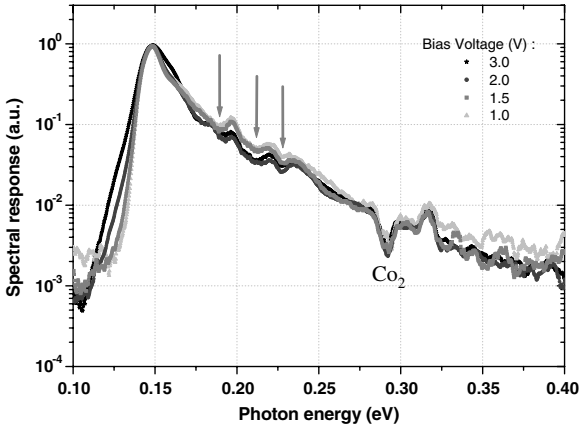

Fig. 3. Experimental Log photocurrent spectra of typical QWIP samples for different applied electric fields (1 V, 1.5 V, 2 V, 3 V). Note the influence of the electric field in the low energy part and the sharp features indicated by continuous arrows in the high energy part.

observed in the high energy part of the spectra as indicated by arrows in Fig. 3. These features show very little dependence on the applied bias. Apart from the well documented $\sin^2\theta$ dependence of the QWIP responsivity [9], no influence of the angle of incidence is observed on these spectral responses. Indeed, measurements have been made for different angles of incidence and we noticed that there was no difference in the shape of the spectral response. We also pointed out that the feature at 280 meV corresponds to a CO_2 residual absorption peak due to the difference in optical way between the signal and the reference channels.

3. Theoretical model of photocurrent spectra

3.1. Kronig–Penney model

Since we are interested in the spectral aspects of the responsivity, we have not included the already well known transport mechanisms such as electric field redistribution in the QWIP structure or carrier injection at the blocking barrier [10,11]. Indeed, these theoretical ingredients are primordial for describing the quantitative photoresponse of QWIP but bring little information on the spectral shape.

Since the features observed are not affected by the electric field, we made the assumption that they are due to the quantum well periodicity and not to any complex quantum effect calling for a complete solution of the Schrödinger equation of this complex structure under an applied electric field. This quantum interference between the periodic quantum wells is known to be the basis of superlattice photodetectors – where quantum well are coupled by tunnelling [12] – but is generally neglected in QWIP modelling. We have thus chosen a simple Kronig–Penney model to describe the states in the quantum wells [13].

First of all, we have to resolve the Schrödinger equation using the respective effective masses of the corresponding materials, in each region of the structure where one period consists in one barrier with a thickness b and a well with a thickness w (see Fig. 4):

$$\frac{-\hbar^2}{2m^*}\Delta\Psi(z) + V\Psi(z) = E\Psi, \tag{1}$$

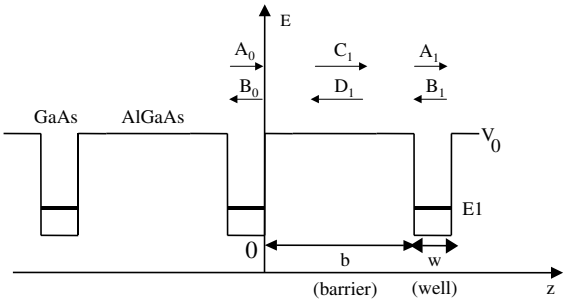

Fig. 4. Multiquantum well structure for the Kronig–Penney model.

where the periodic potential is given by:

$$V = \begin{cases} V_0 & 0 \leqslant z < b, \\ 0 & b \leqslant z < b + w = L. \end{cases} \tag{2}$$

For each part of the structure, the solutions are:

$$\Psi(Z) = \begin{cases} A_0 e^{ikz} + B_0 e^{-ikz} & -w \leqslant z \leqslant 0, \\ C_1 e^{ik_b^{(z-w)}} + D_1 e^{ik_b^{(z-w)}} & 0 \leqslant z \leqslant b, \\ A_1 e^{ik(z-L)} + B_1 e^{-ik(z-L)} & b \leqslant z \leqslant L, \end{cases} \tag{3}$$

where:

$$k = \sqrt{\frac{2m}{\hbar^2}E}, \qquad k_b = \sqrt{\frac{2m_b}{\hbar^2}(E - V_0)}. \tag{4}$$

Using the boundary conditions at $z = 0$, we find the coefficients of the wave functions in region 0 and the barrier b:

$$\begin{bmatrix} C_1 \\ D_1 \end{bmatrix} = \overline{\overline{F}}_{b0} \begin{bmatrix} A_0 \\ B_0 \end{bmatrix}. \tag{5}$$

Similarly, the boundary conditions at $z = b$ give the matrix equation for region 1 and the barrier b:

$$\begin{bmatrix} A_1 \\ B_1 \end{bmatrix} = \overline{\overline{F}}_{1b} \begin{bmatrix} C_1 \\ D_1 \end{bmatrix}. \tag{6}$$

We have the transition matrix for one period consisting of one well and one barrier:

$$\begin{bmatrix} A_1 \\ B_1 \end{bmatrix} = \overline{\overline{T}} \begin{bmatrix} A_0 \\ B_0 \end{bmatrix} \quad \text{where} \quad \overline{\overline{T}} = \overline{\overline{F}}_{1b}\overline{\overline{F}}_{b0}. \tag{7}$$

For the nth period, we find:

$$\begin{bmatrix} A_n \\ B_n \end{bmatrix} = \overline{\overline{T}}^n \begin{bmatrix} A_0 \\ B_0 \end{bmatrix}. \tag{8}$$

The eigenvalues and eigenvectors of the 2×2 matrix T are solutions of the determinantal equation:

$$\overline{\overline{T}} \begin{bmatrix} A_0 \\ B_0 \end{bmatrix} = t \begin{bmatrix} A_0 \\ B_0 \end{bmatrix}. \tag{9}$$

We get that the eigenequation is:

$$\cos(qL) = \cos(kw)\cos(k_b b) - \frac{1}{2}\left(P + \frac{1}{P}\right)\sin(kw)\sin(k_b b) = f_q(E), \tag{10}$$

where:

$$P = \frac{mk_b}{m_b k}.$$

This equation clearly shows that only the energies such that the condition $|f_q(E)| \leqslant 1$ is satisfied will be acceptable (see Fig. 5). The allowed regions are called minibands (see Fig. 6).

The existence of these minibands rather than discrete energy levels, is quite similar to what happens in supperlattice structure.

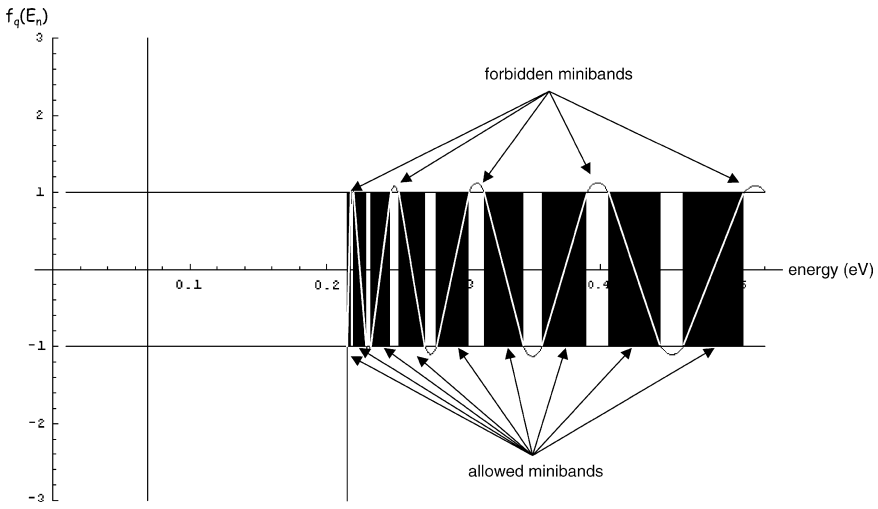

Fig. 5. Plot of the eigenequation $f(E)$ (=$\cos qL$) versus the energy E.

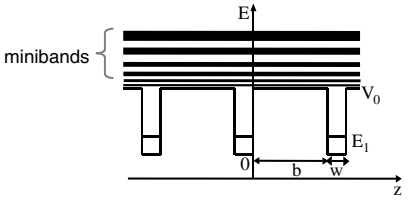

Fig. 6. The so called minibands in a QWIP structure.

Once the structure of the multiquantum well has been described using the Kronig–Penney approach, we can calculate the absorption between the bound state and the minibands. The periodic potential involves that we can work with the Bloch functions. Let $|n,k\rangle$ be the Bloch quantum state of wave vector k in the nth band:

$$|n,k\rangle = u_{n,k}(z)\mathrm{e}^{\mathrm{i}kz}, \tag{11}$$

where the function $u_{n,k}(z)$ displays the periodicity of the QWIP structure, i.e., $u_{n,k}(z+L) = u_{n,k}(z)$.

The momentum matrix element between the bound state $|1,k\rangle$ and the excited state $|n,k'\rangle$ is given by:

$$p_{1n}(k,k') = \left|\left\langle 1,k\left|\frac{A\hat{p}_z}{m}\right|n,k'\right\rangle\right|, \tag{12}$$

where A is the infrared light vector potential, m the electron mass and $\hat{p}_z = (\hbar/\mathrm{i})(\mathrm{d}/\mathrm{d}z)$is the momentum operator which has to be used in periodic structure [9,10]. A straightforward calculation shows that:

$$p_{1n}(k,k') = p_{1n}(k) = \frac{A}{m}\hbar\left|\int u_{1,k}(z)^*\frac{\mathrm{d}}{\mathrm{d}z}u_{n,k}\mathrm{d}z\right|\delta(k,k'), \tag{13}$$

where δ is the Kronecker symbol and $\hbar$ is the Planck constant. The integral is evaluated over a single quantum well period. The Fermi golden rule provides the probability $P(h\nu)$ of the electron excitation by the incident photon flux of energy $h\nu$:

$$P(h\nu) \propto \rho(E1 + h\nu)p_{1,n}(k)^2, \tag{14}$$

where $\rho(E)$ is the density of states in the periodic structure. The absorption spectrum is then the convolution of the excitation probability $P(h\nu)$ with a Lorentzian line shape of broadening parameter Γ:

$$L(h\nu) = \frac{\Gamma}{\pi}\cdot\frac{1}{\Gamma^2 + (E - E1 - h\nu)}. \tag{15}$$

3.2. Interpretation

In order to illustrate the importance of the quantum well periodicity, we have compared (see Fig. 7) the absorption spectrum calculated by our Kronig–Penney approach with the one obtained using expression (10) in Ref. [14] which neglects this periodicity. This graph clearly shows the Van Hove singularities at the miniband edge at high energy whereas this phenomena does not appear in the simulation of the absorption of a single quantum well. We can also notice the sharper cut-off at low energy given by our approach.

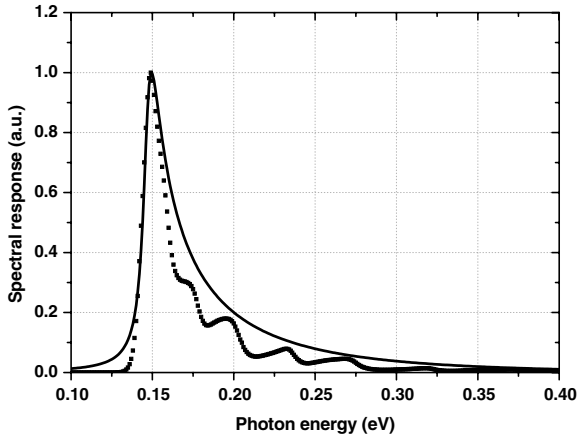

Fig. 7. Comparison between the absorption spectrum of the QWIP calculated in a single quantum well (continuous line) and in a periodic QWIP structure (dotted line). The broadening coefficient is $\Gamma = 5$ meV.

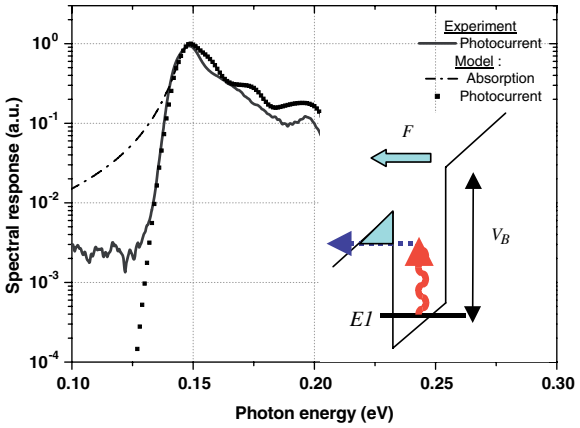

Fig. 8. Comparison between an experimental QWIP Log spectrum (continuous line), the theoretical absorption (dashed line) and the theoretical photocurrent spectra (dotted line) taking into account the electric field assisted tunnelling effect (see inset).

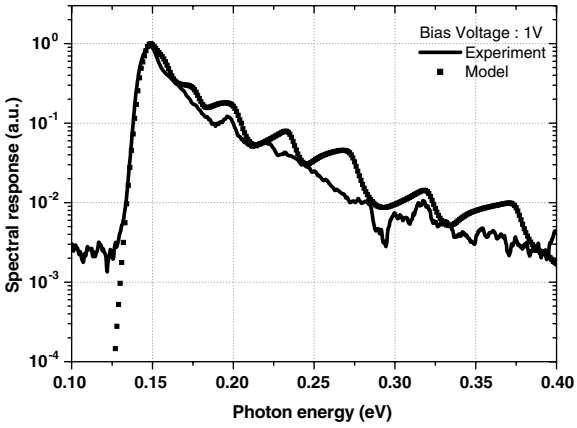

Fig. 9. Comparison between an experimental Log spectrum (continuous line) and our theoretical model taking into account the electric field assisted tunnelling effect and the Van Hove singularities at the miniband edges (dotted line).

The low energy part of the photocurrent spectrum is obtained by requiring that electrons photoexcited below the barrier energy V_B may tunnel through the triangular barrier induced by the electric field using the Fowler–Nordheim transmission coefficient (see expression (4) in Ref. [15] for instance). Fig. 8 shows the comparison in the low energy part between the theoretical absorption, the photocurrent and an experimental Log spectrum respectively. The agreement is convincing and the influence of the Fowler–Nordheim effect is clearly illustrated. Photons with energy below the ionization threshold V_B–E_1 (see inset of Fig. 8) are absorbed but do not yield a photocurrent in the absence of an electric field: This leads to a different cut off in the photocurrent spectrum compared to the absorption one. This cut off is gradually moving toward lower energy with the increasing electric field (Fowler–Nordheim effect) which explains the low energy features of Fig. 3.

This mechanism at low energy has already been mentioned in the QWIP literature concerning the dark current [15], the escape probability from quantum well [16,17] or the injection mechanism at the injecting contact [18]. However, to the best of our knowledge, this feature has not been clearly identified in photocurrent spectra. As far as the high energy part of the Log spectra is concerned, the spectral features are reminiscent of Van Hove singularities.

Fig. 9 shows the comparison between an experimental Log spectrum and our theoretical model, taking into account both Fowler–Nordheim and Van Hove singularities effects. The overall agreement is rather good, particularly concerning the position of the Van Hove singularities. However, two points raise questions: Firstly, there is still an important quantitative discrepancy between our theoretical model and the experimental Log spectra on the high energy side. This discrepancy is most certainly due to different contributions such as the band non parabolicity, and the energy dependent mobility of the free carriers. The second point is the rather low value of the determined broadening coefficient Γ. Indeed, the rather sharp features observed in the Log spectra are compatible with a value of 5 meV but not with the usual value of 10 meV.

4. Summary and conclusions

In conclusion, photocurrent spectra of QWIP devices have been studied over more than three decades. These Log spectra reveal features which have been largely overlooked before.

We have developed an original model. Electric field assisted tunnelling and Van Hove singularities – somewhat reminiscent of quasi-bound states observed by Capasso et al. [19] in electron Fabry–Perot type structures – are the two main phenomena taken into account in this model. These effects are shown to play an important role in the low and high energy parts of the QWIP photocurrent respectively. The off-band photoresponse is found to be non negligible (>1% in the 3–5 μm for a 8–12 μm detector) but smaller than expected by the theory.

Acknowledgements

The authors are also grateful to colleagues from Thales-RT for providing the samples studied here.

References

[1] B.F. Levine, J. Appl. Phys. 74 (1993) R1–R81.
[2] H.C. Liu, B. Levine, J. Andersson (Eds.), Intersubband Transitions in Quantum Wells, Plenum, London, 1994, pp. 97–110.
[3] J.L. Pan, C.G. Fonstad Jr., Mater. Sci. Eng. 28 (2000) 65–147.
[4] K.K. Choi, Physics of Quantum Well Infrared Photodetectors, World Scientific, 1997.
[5] S.D. Gunapala, S.V. Bandara, J.K. Liu, M. Jhabvala, K.K. Choi, Infrared Phys. Technol. 44 (2003) 411–425.
[6] I. Ribet-Mohamed, J. Le Rouzo, S. Rommeluere, M. Tauvy, N. Guérineau, Infrared Phys. Technol. 49 (2005) 119–131.
[7] K.K. Choi, B.F. Levine, R.J. Malik, J. Walker, C.G. Bethea, Phys. Rev. B 35 (1987) 4172–4175.

[8] E. Costard, Ph. Bois, X. Marcadet, A. Nedelcu, Infrared Phys. Technol. 47 (2005) 59–66.
[9] E. Rosencher, B. Vinter, Optoelectronics, Cambridge University Press, Cambridge, 2002.
[10] M. Ershov, C. Hamaguchi, V. Ryzhii, Jpn. J. Appl. Phys. 35 (1996) 1395–1400.
[11] L. Thibaudeau, Ph. Bois, J.Y. Duboz, J. Appl. Phys. 79 (1996) 446–464.
[12] M. Helm, Semicond. Sci. Technol. 10 (1995) 557–575.
[13] S.L. Chuang, Physics of Optoelectronic Devices, Wiley Interscience, New York, 1995.
[14] H.C. Liu, J. Appl. Phys. 73 (1993) 1–7.
[15] S.R. Andrews, B.A. Miller, Appl. Phys. Lett. 70 (1991) 993.
[16] E. Martinet, E. Rosencher, F. Chevoir, J. Nagle, Ph. Bois, Phys. Rev. B 44 (1991) 3157–3161.
[17] B.F. Levine, E. Rosencher, B. Vinter, B.F. Levine (Eds.), Intersubband Transitions in Quantum Wells, Plenum, London, 1992.
[18] E. Rosencher, F. Luc, Ph. Bois, S. Delaitre, Appl. Phys. Lett. 61 (1992) 468–470.
[19] F. Capasso, C. Sirtori, J. Faist, D.L. Sivco, S.-N.G. Chu, A.Y. Cho, Nature 358 (1992) 565–567.